Are rupture zone limits of great subduction earthquakes controlled by upper plate structures? Evidence from MCS data aquired across the Northen Ecuador-South West Colombia margin

J.-Y. Collot, B. Marcaillou, F. Sage, F. Michaud, W. Agudelo, P. Charvis, David Graindorge, Marc-André M-A Gutscher, G. Spence

Are rupture zone limits of great subduction earthquakes controlled by upper plate structures? Evidence from multichannel seismic reflection data acquired across the northern Ecuador–southwest Colombia margin

Jean-Yves Collot,[1] Boris Marcaillou,[2] Françoise Sage,[2] François Michaud,[2] William Agudelo,[2] Philippe Charvis,[1] David Graindorge,[2] Marc-André Gutscher,[3] and George Spence[4]

Received 2 March 2004; revised 18 June 2004; accepted 29 July 2004; published 18 November 2004.

[1] Subduction of the Nazca plate beneath the Ecuador-Colombia margin has produced four megathrust earthquakes during the last century. The 500-km-long rupture zone of the 1906 (M_w = 8.8) event was partially reactivated by three thrust events, in 1942 (M_w = 7.8), 1958 (M_w = 7.7), and 1979 (M_w = 8.2), whose rupture zones abut one another. Multichannel seismic reflection and bathymetric data acquired during the SISTEUR cruise show evidence that the margin wedge is segmented by transverse crustal faults that potentially correlate with the limits of the earthquake coseismic slip zones. The Paleogene-Neogene Jama Quininde and Esmeraldas crustal faults define a ~200-km-long margin crustal block that coincides with the 1942 earthquake rupture zone. Subduction of the buoyant Carnegie Ridge is inferred to partially lock the plate interface along central Ecuador. However, coseismic slip during the 1942 and 1906 earthquakes may have terminated against the subducted northern flank of the ridge. We report on a newly identified Manglares crustal fault that cuts transversally through the margin wedge and correlates with the limit between the 1958 and 1979 rupture zones. During the earthquake cycle the fault is associated with high-stress concentration on the plate interface. An outer basement high, which bounds the margin seaward of the 1958 rupture zone, may act as a deformable buttress to seaward propagation of coseismic slip along a megathrust splay fault. Coseismic uplift of the basement high is interpreted as the cause for the 1958 tsunami. We propose a model of weak transverse faults which reduce coupling between adjacent margin segments, together with a splay fault and an asperity along the plate interface as controlling the seismogenic rupture of the 1958 earthquake. *INDEX TERMS:* 8105 Tectonophysics: Continental margins and sedimentary basins (1212); 8020 Structural Geology: Mechanics; 8005 Structural Geology: Folds and folding; 3025 Marine Geology and Geophysics: Marine seismics (0935); 7209 Seismology: Earthquake dynamics and mechanics; *KEYWORDS:* Ecuador-Colombia, subduction earthquakes, active margin structures, multichannel seismic reflection, morphology

Citation: Collot, J.-Y., B. Marcaillou, F. Sage, F. Michaud, W. Agudelo, P. Charvis, D. Graindorge, M.-A. Gutscher, and G. Spence (2004), Are rupture zone limits of great subduction earthquakes controlled by upper plate structures? Evidence from multichannel seismic reflection data acquired across the northern Ecuador–southwest Colombia margin, *J. Geophys. Res.*, *109*, B11103, doi:10.1029/2004JB003060.

1. Introduction

[2] Great subduction earthquakes nucleate along the seismogenic zone, a relatively shallow portion of the plate boundary interface where subducting and overriding plates are sufficiently coupled to accumulate elastic stress [*Pacheco et al.*, 1993; *Scholz*, 1988]. The occurrence of subduction megathrust events depends mainly on the rheology of the forearc [*McCaffrey*, 1993], the transient shear stress magnitude on the fault [*Wang et al.*, 1995], the thermal structure and width of the coupled zone [*Hyndman and Wang*, 1995; *Kanamori*, 1986], the asperity distribution [*Ruff and Kanamori*, 1983; *Thatcher*, 1990] and physical properties of interplate rocks [*Vrolijk*, 1990; *Moore and Saffer*, 2000]. However, the mechanical factors that control the length and therefore the lateral limits of the brittle rupture are still poorly understood.

[3] Mounting evidence suggests that subducting topographic features, which locally increase interplate coupling

[1]Geosciences Azur, Institut de Recherche pour le Développement, Villefranche sur Mer, France.
[2]Geosciences Azur, Université Pierre et Marie Curie, Villefranche sur Mer, France.
[3]Centre National de la Recherche Scientifique, Université de Bretagne Occidentale, UMR 6538 Domaines Oceaniques, Plouzane, France.
[4]School of Earth and Ocean Sciences, University of Victoria, Victoria, British Columbia, Canada.

0148-0227/04/2004JB003060$09.00

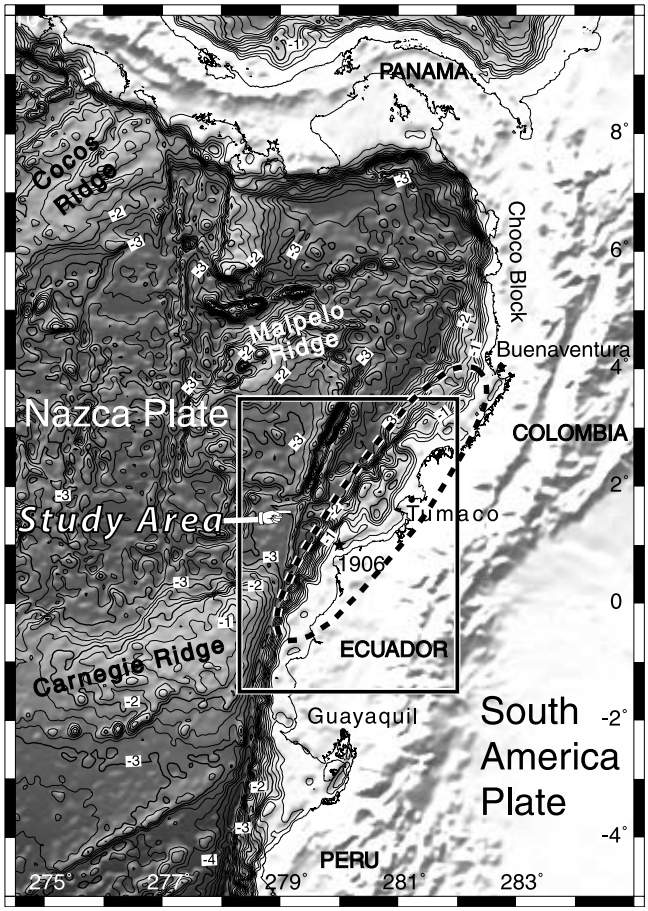

Figure 1. Bathymetric map of the Nazca plate and adjacent North Andean margin derived from satellite altimetry data [*Sandwell and Smith*, 1994]. Location of the study area and estimated rupture zone (dashed line) and epicenter (star) of the 1906 great subduction earthquake [*Kelleher*, 1972] are shown.

[*Cloos and Shreve*, 1996; *Kelleher and McCann*, 1976; *Mogi*, 1969; *Scholz and Small*, 1997], may act as strong interplate asperities rupturing during earthquakes, as recently exemplified along the Costa Rica margin [*Bilek et al.*, 2003; *Husen et al.*, 2002]. Subducting bathymetric highs may also present a barrier to the lateral propagation of a brittle rupture, as shown by a subducting seamount that correlates with the western boundary of the 1946 Nankaido earthquake brittle rupture zone [*Kodaira et al.*, 2000] and an interpreted tear fault in the Philippine Sea Plate that coincides with the eastern boundary of the same event [*Cummins et al.*, 2002]. In addition to subducting features inhibiting lateral rupture propagation, *Mogi* [1969], *Stauder* [1972], and *Sykes* [1971] pointed out that the along-strike boundaries of Japanese and Alaska-Aleutian rupture zones appear to coincide with margin transverse structures.

[4] In the region of northern Ecuador–SW Colombia, the subduction of the Nazca plate beneath South America has produced one of the best examples of variable earthquake rupture behavior [*Kanamori*, 1986; *Kanamori and Given*, 1981; *Thatcher*, 1990]. In 1906, the plate interface ruptured in a single great thrust earthquake (M_w = 8.8) [*Kanamori and Given*, 1981; *Kanamori and McNally*, 1982], with an estimated rupture length of 500 km [*Kelleher*, 1972] (Figure 1). Approximately the same portion of the plate interface ruptured again in three smaller thrust events, directly adjacent to one another [*Mendoza and Dewey*, 1984]. These events occurred from south to north in 1942 (M_w = 7.8) [*Swenson and Beck*, 1996], 1958 (M_w = 7.7) and 1979 (M_w = 8.2) [*Beck and Ruff*, 1984; *Herd et al.*, 1981; *Kanamori and McNally*, 1982] (Figure 2). Their ruptures, including that of the 1906 event, propagated from the SW to the NE end of individual rupture zones [*Kanamori and McNally*, 1982; *Kelleher*, 1972], and are associated with reported tsunamis, with the exception of the 1942 event [*Abe*, 1979; *Espinoza*, 1992; *Kelleher*, 1972].

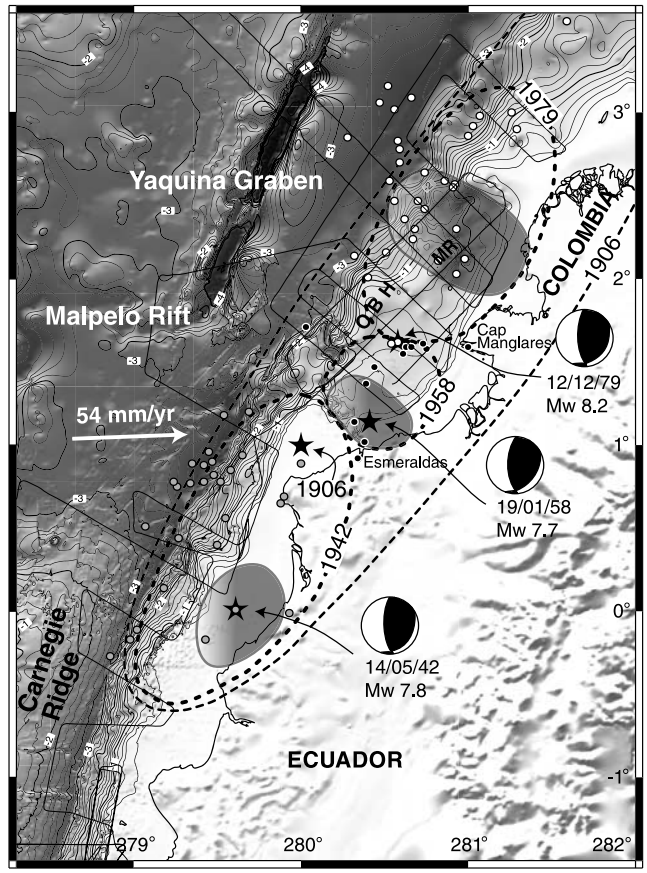

Figure 2. Location of the 20th century great subduction earthquake rupture zones of northern Ecuador–SW Colombia (dashed ellipses), epicenters (stars), and their associated relocated 3-month aftershocks of m_b > 4.8 (white, black, and red dots) [*Mendoza and Dewey*, 1984], seismological asperities (gray shaded elliptic areas) and focal mechanisms [*Kanamori and Given*, 1981; *Kanamori and McNally*, 1982; *Swenson and Beck*, 1996; *Herd et al.*, 1981; *Beck and Ruff*, 1984]. Bathymetry map in km has been compiled from NGDC and the R/V *Nadir* SISTEUR cruise single beam bathymetric data (red lines) and swath bathymetry from the R/V *l'Atalante* Pugu cruise and the R/V *Sonne* Salieri and SO162 cruises. OBH is outer basement high; MR is middle ridge. Open arrow shows Nazca–South America relative plate motion vector, derived from *Trenkamp et al.*'s [2002] GPS study. See color version of this figure at back of this issue.

[5] On the basis of the complexity of the body waveforms produced by large earthquakes, *Kanamori and McNally* [1982] used the simple asperity model of *Lay et al.* [1982] to account for the observed rupture pattern. *Kanamori and McNally* [1982] modeled the 20th century Colombia-Ecuador earthquake sequence by two relatively small asperities (1942, 1958) and a larger one (1979) located respectively at latitudes 0°, 1°15′N, and 2°20′N (Figure 2). This asperity model applies to the rupture zone of the 1942 event within the uncertainty of the teleseismically located aftershocks [*Mendoza and Dewey*, 1984]. The asperity of the 1942 event lies mainly in the southern part of the rupture zone as indicated by the high moment release and observed intensities [*Swenson and Beck*, 1996] (Figure 2). The northern limit of the aftershocks suggests that the 1942 rupture was blocked by the asperity of the 1958 event [*Mendoza and Dewey*, 1984], which indeed acted as a barrier to lateral rupture propagation. In contrast, the asperity model fails to explain the 1958 earthquake because the northward rupture propagation, as defined by relocated aftershocks [*Mendoza and Dewey*, 1984] as well as source time modeling of the 1958 and 1979 earthquakes, indicates rupture was not blocked at the large asperity of the 1979 event but instead ended midway between the two asperities [*Beck and Ruff*, 1984] (Figure 2). This raises the question of the nature of the boundary between the 1958 and 1979 rupture areas and more generally of the boundary between 1942 and 1958 events and extremities of large rupture areas. An additional question relates to the nature of the seaward limit of the 1958 rupture, which, according to modeling of spatial variations in moment release [*Beck and Ruff*, 1984] and the paucity of aftershocks near the trench [*Mendoza and Dewey*, 1984], ceased ~25 km landward from the trench, near the summit of a gentle, outer forearc topographic rise (Figure 2).

[6] In this paper, we address the structural nature of the barriers that potentially block brittle, interplate rupture propagation. Recently acquired marine geophysical data from the rupture zone of the 1906 subduction earthquake are presented here and offer compelling evidence that the northern Ecuador–SW Colombia margin is segmented by transverse crustal faults. We further suggest that, in addition to the subduction of the Carnegie Ridge, a large buoyant oceanic asperity that appears to control the southern limit of the 1906 and 1942 rupture zones, a key transverse crustal fault may be responsible for blocking the lateral propagation of the 1958 brittle rupture zone, and for triggering the 1979 earthquake. Finally, we propose that a major landward dipping, crustal discontinuity of the margin wedge provided a seaward boundary to rupture during the 1958 earthquake.

2. Geophysical Data

[7] Conventional single beam bathymetry data were acquired along the Ecuador-Colombia margin during the SISTEUR experiment conducted during autumn 2000 on board the R/V *Nadir*. We integrate these data with digital bathymetry from National Geophysical Data Center (NGDC) and a few multibeam swath bathymetric lines to produce a new bathymetric compilation (Figure 2), which reveals the general morphology of the entire study area.

[8] Deep penetration multichannel seismic reflection (MCS) data were obtained across the Ecuador-Colombia margin during the SISTEUR cruise [*Collot et al.*, 2002] (Figure 2). MCS data were recorded using a 45-L air gun seismic source tuned in a single bubble mode, and a 360-channel, 4.5-km-long streamer. Shots were fired every 50 m, providing 45-fold coverage. Seismic reflection data were processed using Geovecteur™ seismic processing software to obtain time migrated sections. Processing included common depth point (CDP) gather, high-pass filter, velocity-dependent gain restitution, multiple attenuation in the frequency-wave number (FK) domain, minimum-phase conversion of the signal, external mute, deconvolution, dip move out correction and/or normal moveout correction, internal mute, time variant band-pass filter, stack, deconvolution, and Kirchhoff migration. The final plots included a filter in the FK domain, and a time variant dynamic equalization. Depth values are given for specific reflectors on the basis of velocities derived from wide-angle seismic data collected during the SISTEUR cruise [*Agudelo et al.*, 2002; *Graindorge et al.*, 2004].

3. Morphology of the Northern Ecuador–SW Colombia Margin and Its Correlation to Limits Between Great Earthquake Rupture Zones

[9] Previous studies have shown that the Ecuador margin is erosional [*Collot et al.*, 2002; *Moberly et al.*, 1982] and is segmented on a large scale as a result of the Carnegie Ridge subduction [*Gutscher et al.*, 1999], whereas the Colombia margin is dominantly accretionary [*Westbrook et al.*, 1995; *Marcaillou*, 2003]. Near latitude 1°30′N, the Ecuador–SW Colombia margin shows a sharp along-strike change in morphology [*Gutscher et al.*, 1999] (Figure 2) and gravity anomalies (Figure 3) at the Esmeraldas canyon. This active canyon deeply incises the margin along its N140°E trending upper course that separates margin segments with strongly contrasting morphologies. South of the canyon, the margin segment shows a shallow (<100 m), up to 50-km-wide continental shelf, a steep (~14°) and short (20–30 km) inner trench slope, near zero free-air gravity anomalies, and an uplifted coastline documented by Quaternary marine terraces [*Pedoja*, 2003]. At the junction with the Carnegie Ridge, the Ecuador trench shallows to 2880 m and contains only few meters of turbidite [*Lonsdale*, 1978], whereas it deepens to 4000 m and contains up to 500 m of sedimentary fill west of the Esmeraldas canyon [*Collot et al.*, 2002]. Although there is no clear evidence for a correlation between the morphology of this margin segment and the southern limit of the 1906–1942 rupture zones, it is worth noting that this limit correlates closely with the shallowest trench segment (Figure 2) and with a N65°E trending gravity low (Figure 3), which outlines the transition from the shelf near-zero free-air anomaly (FAA) to >50 mGal gravity values farther south.

[10] North of the Esmeraldas canyon, the margin is marked by a narrow (5–20 km) shelf, and a remarkable, up to 80-km-wide, 800- to 1000-m-deep morphologic reentrant, containing a sedimentary forearc basin. The forearc basin is bounded seaward by a 50-km-long outer basement high overhanging the trench at longitude 280° 25′, and a middle ridge at longitude 280° 50′ that rises to a water depths of 60 m [*Marcaillou*, 2003]. The reentrant and

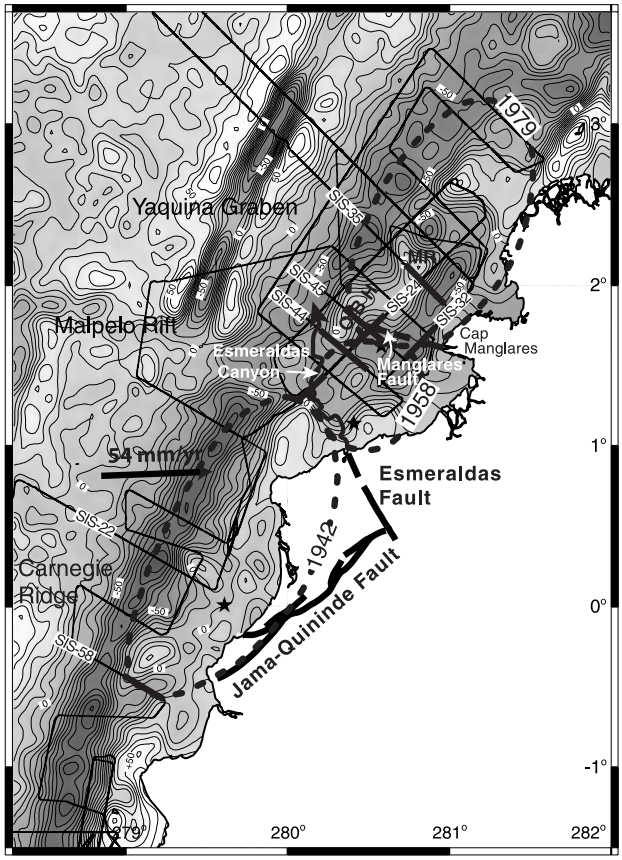

Figure 3. Satellite-derived free-air gravity anomaly along the northern Ecuador–SW Colombia margin [*Sandwell and Smith*, 1994]. Contours are every 10 mGal. Stars and dashed lines are locations of great subduction earthquake epicenters and rupture zones. OBH is outer basement high; MR is middle ridge. Main fault systems are shown onshore [*Deniaud*, 2000; *Zamora et al.*, 1993]. Thin lines are ship tracks of the SISTEUR cruise. MCS data used in this study are shown as heavy dark lines with labels.

ridges are associated with −70 mGal and +20 mGal FAA, respectively. The Colombia trench, which locally contains up to 3.5 km of turbidites [*Collot et al.*, 2002; *Marcaillou*, 2003], bounds the margin seaward, whereas a subsiding coast dominated by mangroves and estuarine deposits flank the margin landward [*Deniaud*, 2000].

[11] The boundary between the margin segments north and south of the Esmeraldas canyon is outlined by a NE facing, 1000-m-high morphologic scarp characterized by a steep gravity gradient (5 mGal/km). This major scarp coincides with the area where 1942 and 1958 earthquake rupture zones abut one another. Only minor morphologic and gravity anomaly changes (Figures 2 and 3) characterize the boundary between the 1958 and 1979 earthquake rupture zones.

4. Crustal Structures at the Boundaries Between Great Earthquake Rupture Zones

[12] Deep seismic reflection lines are used to image the crustal structure of the Ecuador-Colombia margin wedge near the interpreted rupture boundaries between the great subduction earthquakes of the 20th century.

4.1. Southern Limit of 1942 and 1906 Earthquakes

[13] Seismic profile SIS-58 cuts across the Ecuador margin near the southern limit of the 1942 rupture zone, which potentially coincides with that of the 1906 earthquake (Figure 4). The line shows that the margin is underlain by a highly irregular and strongly reflective horizon B, which underlines the base of a well-developed sedimentary basin extending across the continental shelf. The basin consists of three reflective and well-stratified sequences separated by unconformities and overlain by a thin blanket of recent sediments. At CDP 7300, the lower sequence (ls) is vertically offset by ~500 m along a steeply dipping fault. The fault activity has been recorded on its down-thrown side by a rotational sedimentary basin (ms). This activity stopped prior to deposition of the upper sequence (us), as indicated by the undisturbed strata overlaying a major unconformity. Secondary faults appear to have deformed the lower and middle sequences landward of the main fault. Seismic evidence indicates that the faults coalesce downward and

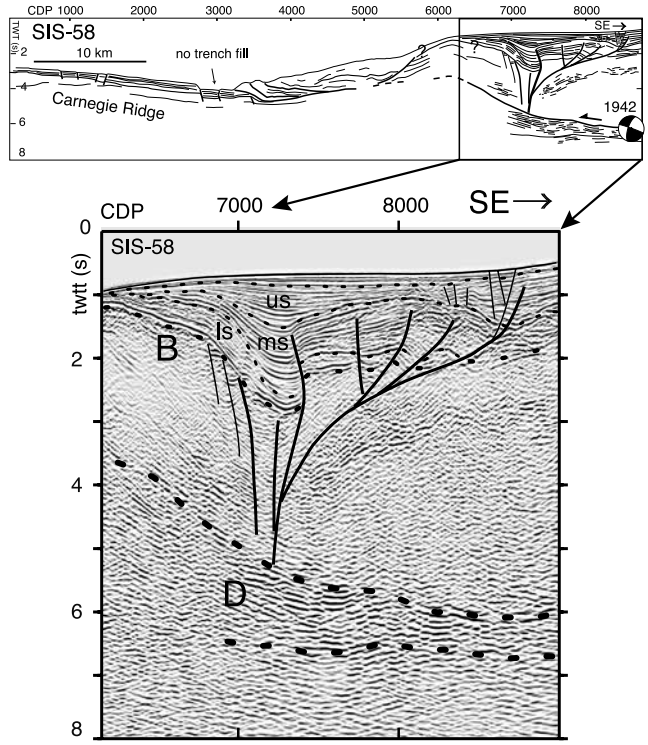

Figure 4. Multichannel seismic reflection line SIS-58 across the Ecuador margin, where the Carnegie Ridge crest is being subducted. Location is shown in Figure 3. (top) Line drawing. The 1942 focal mechanism, situated at a depth of ~14 km [*Swenson and Beck*, 1996], has been projected onto the line, where it matches well with the ~13 km depth of the plate interface according to seismic reflection and wide-angle data. (bottom) Seismic reflection data showing the shelf basin and crustal strike-slip fault system. Abbreviations are as follows: ls is lower sedimentary sequence, ms is middle sequence, and us is upper sequence. B is top of margin basement. D is reflective strata from the top of underthrust Carnegie Ridge.

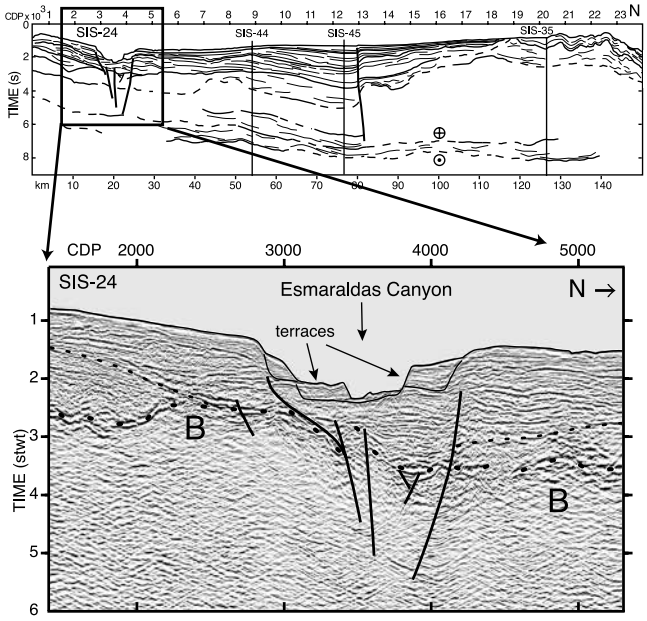

Figure 5. Multichannel seismic reflection strike line SIS-24 across the Esmeraldas canyon. Location is shown in Figure 3. (top) Line drawing. (bottom) Close-ups across offshore segment of the Esmeraldas fault zone. B is basement reflection.

extend into the margin basement. Strongly energetic reflections from within the basement form horizons that dip consistently from both sides of the main fault, toward its downward projection, suggesting a ''flower structure''-type fault pattern. The interpreted fault terminates at depth against a strongly reflective, well-bedded, eastward dipping layer D, which we interpret as Carnegie Ridge strata thrust eastward beneath the margin. On the basis of wide-angle seismic data [*Graindorge et al.*, 2004], the main subvertical fault intersects the top of the subducting plate at a depth of ~10 km. Therefore a major crustal transtensional strike-slip fault, trending NE-ward as indicated by gravity FAA (Figure 3) and imaged on seismic reflection lines from Petroproduccion, deformed the margin during deposition of the midsequence. Onshore geology indicates that this fault represents the seaward projection of the major dextral strike-slip Jama-Quininde fault system (Figure 3), which has been active from the early Paleogene to the Neogene times [*Deniaud*, 2000]. Onshore stratigraphic observations indicate that the Jama-Quininde fault is sealed by upper Miocene deposits [*Deniaud*, 2000]. We conclude that the Jama-Quininde fault system is a major upper plate mechanical discontinuity that divides the margin obliquely. Its offshore continuation coincides roughly with the southern limit of the 1942 earthquake rupture zone.

4.2. Limit Between 1942 and 1958 Earthquake Rupture Zones

[14] The crustal structure associated with the limit between the 1942 and 1958 rupture zones can be interpreted from strike line SIS-24, where it crosses the Esmeraldas canyon (Figure 5). Although the morphologic imprint of the canyon and its associated submarine terraces slightly obscure shallow structures, a strong amplitude, low-frequency basement reflector B deepens north from 2.6 to 3.6 s TWT beneath the canyon and is vertically offset by high-angle faults (Figure 5). The basement offset supports uplift of the Esmeraldas platform relative to subsidence of the margin reentrant. The fault system lies along the upper course of the Esmeraldas canyon, which coincides with the offshore projection of the WNW trending Esmeraldas fault (Figure 3). Because of morphologic complexities, the fault activity cannot be ascertained from marine data. Onshore, the Esmeraldas fault, which dips south, was active from the late Cretaceous-Paleogene to the Neogene time as an extensional structure with minor left-lateral strike slip [*Daly*, 1989; *Deniaud*, 2000]. Therefore the boundary between the 1942 and 1958 rupture zones coincides with the Esmeraldas fault zone.

4.3. Limit Between 1958 and 1979 Earthquake Rupture Zones

[15] Seismic reflection lines SIS-24 and SIS-32 that cut across the interpreted boundary between the 1958 and 1979 earthquake rupture zones (Figure 3) provide evidence for a major crustal fault cutting transversely across the forearc basin. On line SIS-24 (Figure 6), the forearc basin reaches ~4 km in thickness at the depot center, as indicated by well-bedded reflections returned from the basin strata. Near the depot center, at CDP 12800, the basement steps down southward by ~0.8 s TWT across a major high-angle fault. The fault is marked by sharp reflection disruptions and terminations. The fault extends down to ~6.6 s TWT, where it terminates at a set of low-frequency, flat laying reflectors. On the basis of correlations with cross lines SIS-45 and SIS-44 (Figure 3), we believe that the flat laying reflectors SF, De, and To (Figure 6) are associated with a major thrust fault, the plate interface, and the top of the underthrust Nazca plate oceanic crust, respectively. The geometry of the basin strata helps constrain the timing of the fault activity. The deepest, subhorizontal, unconformable, strata of the lower sequence (ls) imply sediment deposition on a paleotopography, suggesting that basement tectonics had started prior to basin sedimentation. Correlation with onshore forearc geology shows that the fault activity could have started by late Paleogene–early Neogene time or earlier [*Evans and Wittaker*, 1982]. The fault was, however, minimally active during deposition of the lower sequence (ls) as indicated by its similar thicknesses across the fault. Fault activity increased during deposition of the midsequence (ms) until the recent times (us), as shown by the twofold thickness of sediments recently deposited on the down-thrown side of the fault. A 10-m-high bathymetric scarp associated with the structural down warping of the basin (Figure 6) supports the recent fault activity. The reverse component of the upper segment of the fault, together with the steep dip of its deeper portion, suggests that the fault is dominantly transpressive.

[16] Line SIS-32 is a strike line that extends immediately offshore Cap Manglares (Figure 3). The line shows that the forearc basin contains as much as ~6 km of stratified, reflective to poorly coherent stratas (Figure 7). Near CDP 7000, the deep section of basin sediment abuts northward against the relatively uplifted southern termination of the acoustic basement B, supporting the presence of an ancient topography or basement fault system. The fault system, which does not have clear shallow and seafloor expressions,

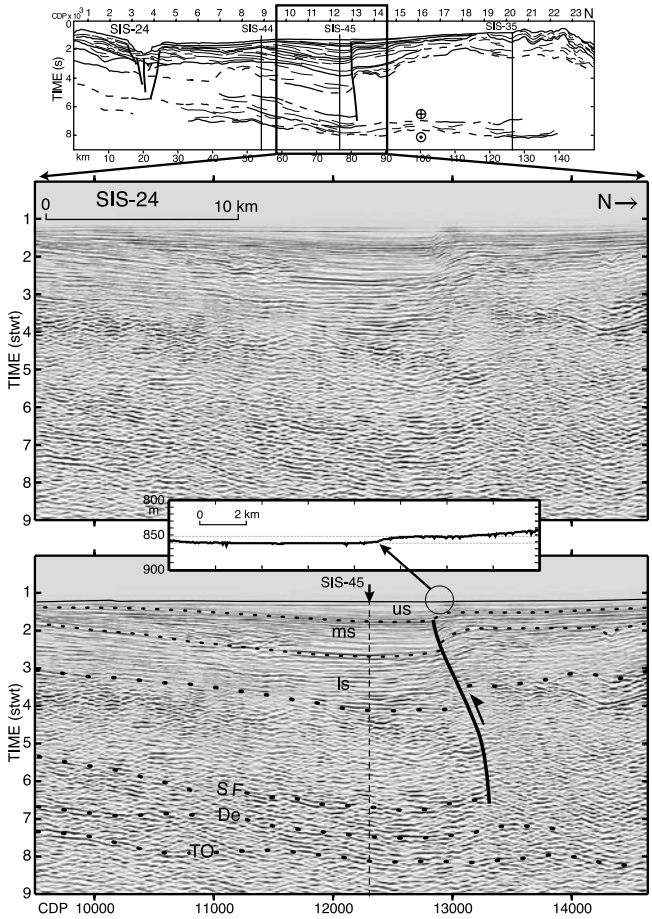

Figure 6. Multichannel seismic reflection strike line SIS-24 across the Manglares fault. Location is shown in Figure 3. (top) Line drawing. (middle and bottom) Close-up across the high-angle Manglares fault. Abbreviations are as follows: ls is lower sedimentary sequence, ms is middle sequence, and us is upper sequence. SF is a splay fault, De is the interplate décollement, and TO is top of oceanic crust as interpreted from cross-seismic lines. Inset is narrow beam bathymetric profile showing a 10-m vertical offset associated with the fault.

may have been dominantly active prior or during deposition of the oldest basin strata. Recent motion of low amplitude is not, however, to be excluded because of sharp basin reflector terminations, small vertical offsets and patches of fuzzy reflections in the sediments overlaying the buried basement fault scarp.

[17] Taken collectively seismic lines SIS-24 and SIS-32 provide evidence for a major, N106°E trending inherited crustal fault, that we named the Manglares fault (Figure 3). The westernmost part of the fault has remained active with an apparent transpressive component on line SIS-24. The Manglares fault, which appears to project seaward from Cap Manglares, at the extremity of a N105°E rectilinear coastline segment, coincides roughly with the limit between the rupture zones of the 1958 and 1979 earthquakes.

4.4. Seaward Limit of 1958 Rupture Zone

[18] Line SIS-44 cuts across the margin wedge ruptured during the 1958 earthquake. Near CDP 9500, the line shows a summit graben that is associated with a gentle rise of both the seafloor and the underlying basement (B in Figure 8). Forearc basin strata beneath the flanks of the seafloor rise dip away from the rise summit and are down dropped along normal faults in the graben. These pieces of evidence demonstrate that the rise and associated deformation result from a compressive upward bulging of the underlying basement, followed by summit extensional collapse. The rough topography of the graben and its absence of sediment fill support active deformation. Compressive deformation may, however, be associated with thinning of the fore margin crust as reflected by the trenchward tilt of the basin section located seaward of the graben.

[19] At depth, line SIS-44 reveals two low-frequency, discontinuous reflections (De and To in Figure 8) that can be traced landward for ~45 km from the deformation front, where they meet each other at a depth of ~7.5 s TWT (~14 km). According to their geometry and depths, these reflections are interpreted as the plate interface (De) and the top of subducted oceanic crust (To). The line also shows a drastic change in the seismic character of the reflections returned from the margin basement across the discontinuous, steeply landward dipping reflector SF. The seismic character changes from subcontinuous, reflective and landward dipping in a wedge of rock underlying reflector SF between CDPs 6500 and 8800, to largely incoherent east of SF (approximately CDP 5000) and west of the wedge (approximately CDPs 8800–9400). Some high-frequency, shallow, landward dipping events are interpreted as multiple (Mu) that could not be removed by multiple attenuation in the FK domain, the apparent velocities of the multiple events being in this case close to apparent velocities of the real ones located at the same depth. We interpret reflector SF as a major crustal discontinuity between margin rocks of different nature or physical properties. SF appears to be branching upward from the plate interface at a depth of ~13 km beneath the seafloor and a distance of ~42 km from the trench. The seaward extent of SF within the compressively deformed, upward bulging basement, supports activation of the SF crustal discontinuity as a thrust fault. SF could thus act as a megathrust splay fault that would decouple the bulk of the margin basement from its frontal part during great earthquake rupture.

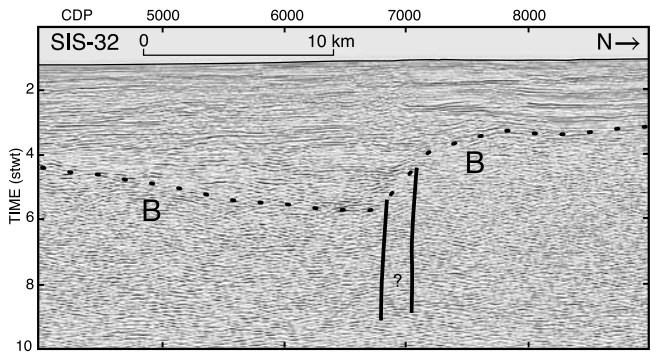

Figure 7. Multichannel seismic reflection strike line SIS-32 along the forearc basin. Location is shown in Figure 3. The line shows a thick sedimentary fill overlying a deformed basement B.

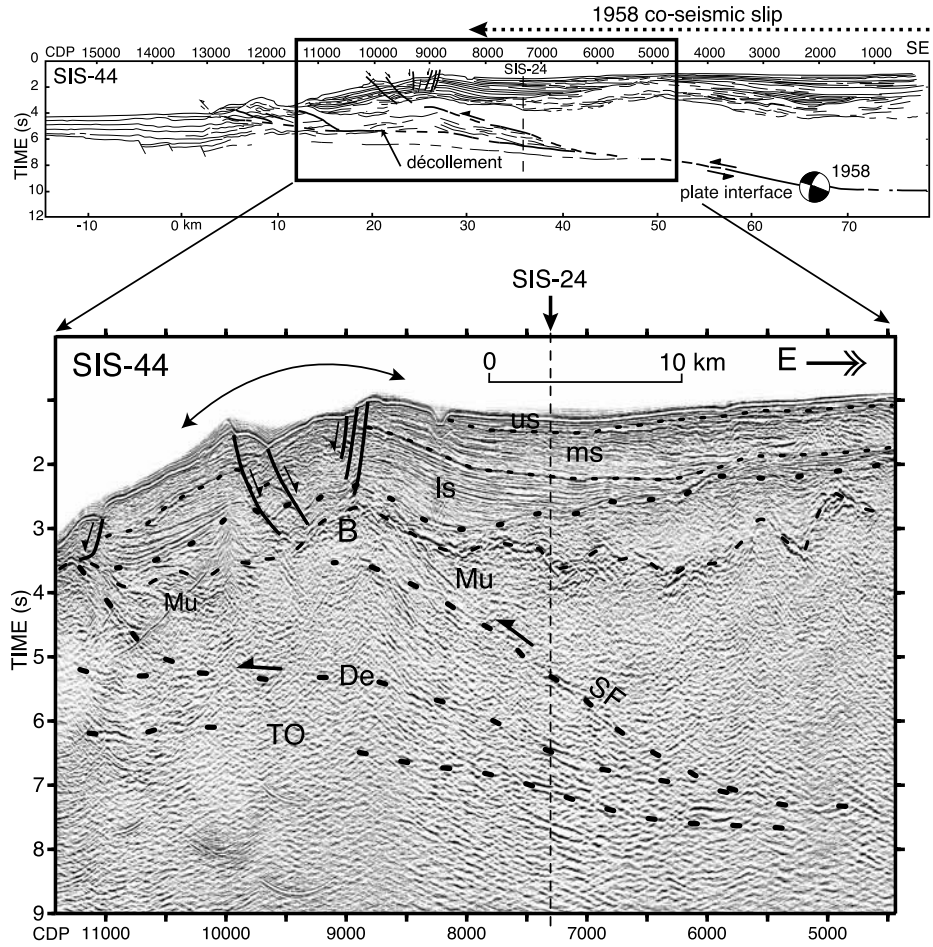

Figure 8. Multichannel seismic reflection line SIS-44 across the margin wedge. Location is shown in Figure 3. (top) Line drawing. Note that the seaward extent of 1958 coseismic slip matches with the frontal bulge and interpreted splay fault. The 1958 focal mechanism, which is similar to that of the 1979 event [*Mendoza and Dewey*, 1984] is projected onto the line at a depth chosen to coincide with the plate interface observed in seismic reflection profiles. (bottom) Close-up showing the forearc basin summit graben associated with a gentle rise of seafloor and underlying basement B. Note difference in basement reflectivity across SF fault. Mu is multiples; ls, ms, us, De, and TO are as in Figure 6.

[20] Although the chronology is uncertain, the geometric relationships between deformed forearc basin units may help to pinpoint SF tectonic activity. The area of the basement bulge was a dual depot center during deposition of the basin lower sequence (ls), as indicated by two adjacent depot centers now tilted away from the bulge axis (approximately CDPs 8200 and 10800). By the time of the middle sequence (ms) deposition, the eastern depot center had migrated landward as indicated by the gentle eastward thickening of the unit, suggesting that bulging had likely started during deposition of the ms unit. The absence of a strong unconformity between ls and ms indicates, however, that the uplift had been moderate. A shallow unconformity between the middle (ms) and upper (us) sequences beneath the present-day depot center supports recent uplift at the seafloor rise, possibly related to SF fault activity.

[21] Seismic reflection line SIS-45 provides evidence for a major subvertical crustal fault "VF" and possibly for fault SF near the junction between the 1958 and 1979 earthquake rupture zones (Figure 9). The line shows the massive outer basement high adjacent to the subsiding forearc basin containing up to 3.4 km of reflective and well-bedded sedimentary strata. The strata are gently tilted eastward, and terminate abruptly westward at a subvertical acoustic boundary, against which they are upwarped. We interpret the acoustic boundary at CDP 7500 as the high-angle active fault VF, which pushed up the outer basement high, and depressed and tilted eastward the forearc basin. Although diffracted energy partially obscures the acoustic signal at depth beneath the interpreted fault, variable reflectivity and discontinuous reflections returned from within the basement underlying the western boundary of the forearc basin is evidence for the downward projection of the fault. Fault VF extends at depth, possibly down to ~5.5 s TWT, where it encounters gently landward dipping reflections. From correlation with strike line SIS-24 (Figure 6) and line SIS-44 (Figure 8), we interpret the deep reflections as the plate interface "De" and top of subducting oceanic crust "To". A steeper subdued reflection, shallower than reflector De beneath the basin, crosses line SIS-24 at 6.5 s TWT and is therefore tentatively

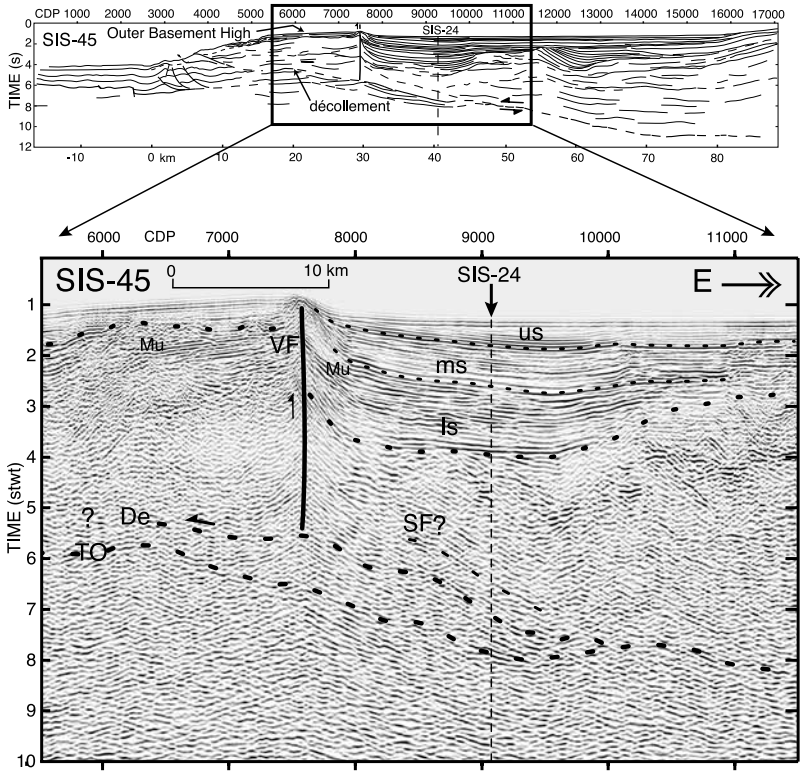

Figure 9. Multichannel seismic reflection line SIS-45 across the outer basement high and forearc basin. Location is shown in Figure 3. (top) Line drawing. (bottom) Close-up showing the flat-topped outer basement high separated from the thick forearc basin by steep fault VF. Mu is a multiple; ls, ms, us, SF, De, and TO are as in Figure 6.

correlated with fault SF. Fault VF would have experienced transpressive motion with regards to its high-angle dip and basin tilt away from the fault.

4.5. Section Across the 1979 Asperity

[22] Seismic reflection line SIS-35 cuts across the middle ridge and 1979 earthquake rupture zone (Figure 3). The line shows that the bathymetry and internal structures differ markedly from those observed farther south on lines SIS-44 and SIS-45. On line SIS-35, the middle ridge culminates at a water depth of 250 m, 42 km from the trench (Figure 10). Folds and high-angle landward dipping reverse faults deform the uppermost basement and the overlying sedimentary forearc basin units, which have been tilted significantly landward. The overall structure supports ridge uplift by strong tectonic shortening distributed across most of the outer forearc. Tectonic activity persists, as indicated by a deformed, recent unconformity (Er in Figure 10) and the bumpy topography associated with anticline axis.

5. Discussion

[23] On a larger scale, although the 500-km rupture length of the 1906 earthquake is subject to some uncertainty, *Kelleher* [1972] and *Kanamori and McNally* [1982] reported that the rupture extended to the Carnegie Ridge-trench intersection, and to the sharp bend of the trench at 4°N (Figure 1). This change in trench orientation from NE to north results from the accretion of the Choco island arc block [*Duque-Caro*, 1990; *Taboada et al.*, 2000] and reflects a change in stress field along the plate interface, capable of blocking the coseismic slip. These characteristics define a geometric barrier such as defined by *Aki* [1979]. *Kelleher*'s [1972] and *Kanamori and McNally*'s [1982] observations also suggest that the rupture propagation of a megathrust earthquake can alternatively be stopped by strong interplate coupling related to subduction of a large feature, such as the Carnegie Ridge. However, for subduction earthquakes of M_w 7.7 to 8.2, structural data presented above demonstrate that their rupture zone limits correlate with interplate seismological asperities and/or barrier-like transverse crustal faults that segment the margin into 100- to 200-km-long blocks (Figure 11). In the sections below, we discuss the influence of the Carnegie Ridge subduction and margin wedge crustal faults on the spatial distribution of earthquake brittle rupture, and propose a model, which accounts for delimiting the rupture propagation of an earthquake of M_w up to 7.7, by a mega thrust splay fault and crustal faults transverse to the margin wedge.

5.1. Carnegie Ridge: A Mega-asperity Bounding Megathrust Ruptures

[24] The Carnegie ridge is a ~300-km-wide Neogene oceanic plateau that resulted from the interaction between the Galapagos hot spot and the Cocos-Nazca spreading center [*Lonsdale*, 1978]. Immediately west of the trench, the ridge is asymmetric in a N-S cross section. With respect to the ridge crest, the ridge shows a 100-km-wide,

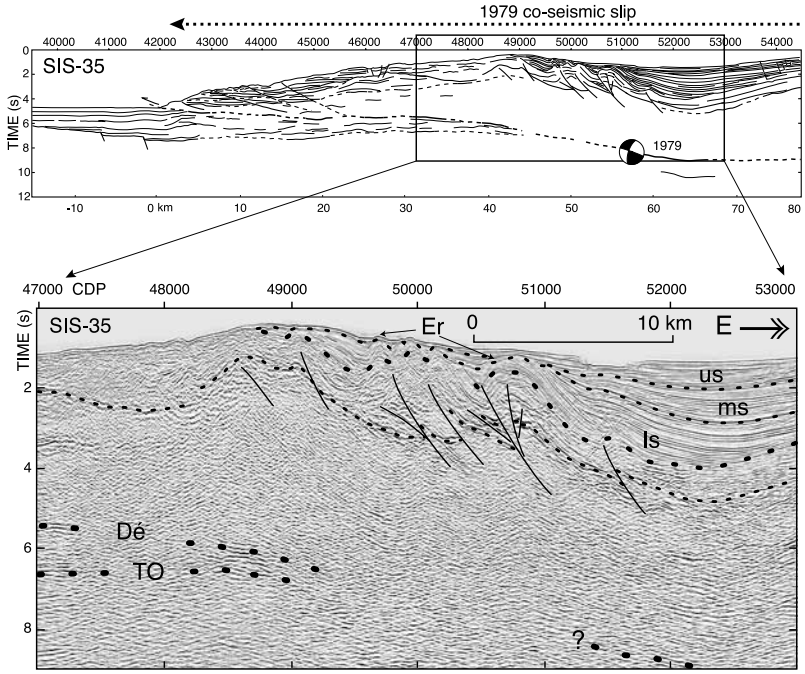

Figure 10. Multichannel seismic reflection line SIS-35 across the middle ridge and forearc basin. Location is shown in Figure 3. (top) Line drawing with cross-margin extent of 1979 coseismic slip. The 1979 focal mechanism [*Kanamori and McNally*, 1982] has been projected onto the line at a depth chosen to coincide with the plate interface according to seismic reflection data. (bottom) Close-up showing shortening distributed across the margin wedge and forearc basin. Er is a recent unconformity; ls, ms, us, De, and TO are as in Figure 6.

steep northern flank, and a ~200-km-wide body and more gentle southern flank. On the basis of wide-angle seismic data, the crust beneath the ridge crest is 19 km thick [*Sallares et al.*, 2002] and 14 km at its southern flank. This thickened oceanic crust can be imaged underthrusting the margin as far as the coast line [*Graindorge et al.*, 2004]. The ridge crest can be traced landward through the trench saddle at 0°20s, toward the onshore drainage divide, allowing us to extrapolate the ridge northern flank beneath the Ecuador margin (Figure 11). Seismic reflection data confirm that, near the northern flank of the Carnegie Ridge, the plate interface shallows southward by ~1.3 km (0.9°) between lines SIS-22 and SIS-58 (Figure 3). Hence this segment of the plate interface is consistent with a southward verging ramp fault that separates volcanic basement rocks of the margin [*Reynaud et al.*, 1999] from subducting ridge sediment dominated by Pleistocene foraminifer and nannofossil ooze, and ash [*Shipboard Scientific Party*, 2002] (Figure 4). The ramp fault and associated buried ridge crest would contribute to blocking the southward propagation of great interplate ruptures. GPS measurements suggest that the margin segment facing the Carnegie Ridge is 50% locked [*Trenkamp et al.*, 2002]. Higher interplate pressure due to the buoyancy of the bulk of the subducted ridge would be responsible for partial locking of the plate interface [*Graindorge et al.*, 2004] and for stopping the 1906 and 1942 rupture zones propagation near the subducted ridge crest. Notwithstanding the main influence of the Carnegie Ridge, the offshore extension of the Jama-Quininde fault (Figure 11) may contribute to blocking the southward rupture propagation along the plate interface by a mechanism discussed below for the Manglares fault.

5.2. Manglares Fault: A Barrier Between the 1958 and 1979 Earthquake Rupture Zones

[25] The N106°E trending Manglares fault is a major crustal transfer fault that separates margin segments with drastically different tectonic regimes as expressed by the wide and largely nondeforming forearc basin south of the fault (line SIS-45, Figure 9) and the severely shortened margin north of the fault (SIS-35, Figure 10). As suggested by seafloor reflectivity (Figure 12, courtesy G. Westbrook), the Manglares fault appears, however, to terminate abruptly westward against the N30°E trending faulted eastern flank of the outer basement high (fault VF in Figure 9) Indeed, GLORIA-derived seafloor reflectivity clearly indicates the trace fault VF but does not image that of the Manglares fault, perhaps because it is associated with a gentle, only 10-m-high variation in seafloor depth (Figure 6).

[26] The Manglares fault is located with 100-m precision on the GPS-calibrated SISTEUR seismic lines. The 1979 epicenter, and the 1958 aftershocks of $m_b > 5.2$ that define the barrier between the 1958 and 1979 rupture zones, appear to cluster along a N100°E direction,10–15 km south of the inferred Manglares fault. The aftershocks were relocated by using the joint hypocenter determination method to minimize errors in the relative locations of the hypocenters [*Mendoza and Dewey*, 1984]. Their 90% confidence error ellipses relative to a calibration event show semiaxes smaller than 20 km. On the basis of this precision and the

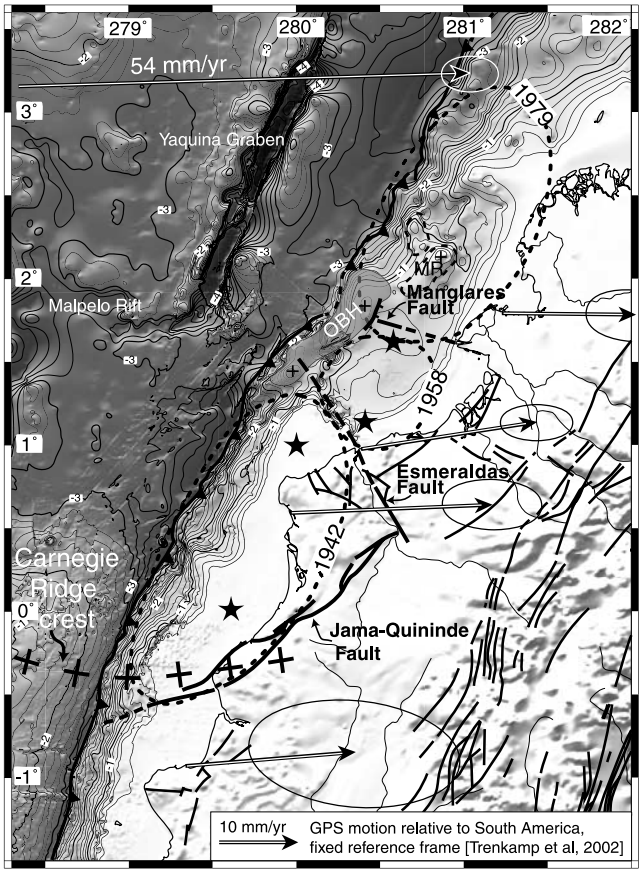

Figure 11. Structural relationships between transverse crustal faults and great earthquake rupture zones. Faults are from *Zamora et al.* [1993] and *Santana and Dumont* [2002]. Crosses represent the Carnegie Ridge crest, which is associated with the offshore extension of the Jama Quininde fault and the southern termination of the 1906 and 1942 earthquake rupture zones. Note that the 1958 earthquake rupture zone is bounded by the Esmeraldas fault, the Manglares fault, and the outer basement high (OBH). Discrepancy between Manglares fault and limit between 1958 and 1979 rupture zones is discussed in text. The location of the Malpelo GPS vector (54 mm/yr) has been shifted to fit in figure.

distance between the hypocenters and the Manglares fault, we consider that the northernmost 1958 aftershocks and the Manglares fault are geographically related. However, based on P wave first motions, the 1958 aftershocks occurred along the plate interface that was ruptured during the 1979 event [*Mendoza and Dewey*, 1984], and not on the Manglares fault itself.

[27] On the basis of the spatial association of the boundary between the 1958 and 1979 rupture zones with the adjacent extinct Malpelo rift and associated Yaquina graben transform fault (Figure 2) [*Lonsdale*, 1978; *Lonsdale and Klitgord*, 1978], *Mendoza and Dewey* [1984] interpreted the seismological barrier as resulting from heterogeneities in the subducting Nazca plate. Our bathymetric compilation (Figure 2) shows that a relative seafloor high, involving small-sized seamounts and oceanic horsts, extends between the trench and Malpelo rift, suggesting that minor oceanic relief is being subducted beneath the margin segment ruptured in 1958. Similar seamounts might be responsible for the 1958 earthquake asperity. However, source time functions models for the 1958 and 1979 events do not require a major fault plane asperity associated with their common rupture boundary (Figure 2) [*Beck and Ruff*, 1984], and seismic reflection data do not provide support for a large subducting seamount near the Manglares fault [*Marcaillou*, 2003]. Alternatively, *Mendoza and Dewey* [1984] suggested that the barrier could result from a minor vertical offset between two fault planes of similar orientations. Considering that the fault planes belong to the plate interface, such an offset could reflect a tear in the down going plate. A tear separating a steeper plate interface south of the Manglares fault from a shallower one to the north could account for the observed deformations at the Manglares fault. Our seismic data, however, do not show evidence for slab distortion or slab tear, neither at depth in the region of the Manglares fault nor beneath the trench. Thus, notwithstanding the key role played by lower plate relief on earthquake ruptures [*Bilek et al.*, 2003; *Dominguez et al.*, 1998; *Scholz and Small*, 1997], we believe that the upper plate transverse Manglares fault may act as a barrier to rupture propagation of subduction earthquakes. The juxtaposition of both, subducting oceanic relief and the

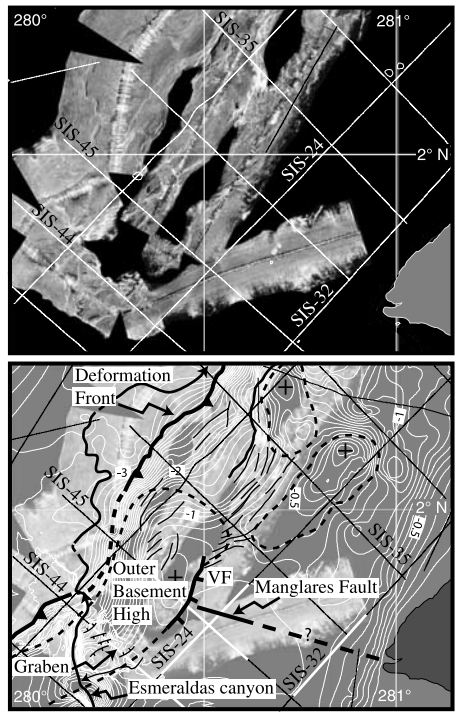

Figure 12. (top) GLORIA side-scan sonar imagery west of Cap Manglares (G. Westbrook personal communication, 2003) with track lines of SISTEUR cruise. White is high reflective seafloor. (bottom) Structural interpretation and bathymetry in km overlay of side-scan sonar imagery. Note that the deformation front, the Esmeraldas canyon/channel, and the fault scarp VF are reflective, whereas the seafloor expression of the Manglares fault is not clearly visible on GLORIA imagery.

Manglares fault would however increase the effect of the fault on the separation on the rupture zones.

5.3. Faulted Outer Basement High: A Frontal Buttress to Earthquake Rupture Propagation

[28] The outer basement high located between the trench and the seaward limit of the 1958 earthquake rupture zone consists of a ~9-km-thick, crustal block bounded by active crustal faults (Figure 11). The block, which appears to be massive on line SIS-45 (Figure 9), has undergone uplift and subsidence. Its flat top, which resembles a wave-cut terrace, and its thin and reflective sedimentary cap suggest that the block was uplifted to sea level and eroded. Uplift may have been accomplished along transpressive fault VF, relative to the subsiding landward margin basement. The block then subsided by ~700–1000 m, as indicated by its present-day water depth. The block subsidence accompanied the overall margin subsidence recorded in the forearc basin. These observations show that, although the outer basement high and adjacent margin basement experienced a complex history of vertical motions, they remained strongly coupled across fault VF and accommodated little shortening. On the basis of the gravity anomaly map (Figure 3), the outer basement high can be extended southward in the region adjacent to the 1958 earthquake rupture zone (Figure 11). On line SIS-44 (Figure 8), the block becomes buried beneath forearc basin strata, undergoes transverse compression and is potentially detached from the margin along the interpreted splay fault acting as a roof thrust. Such a crustal splay fault has been interpreted to accommodate elastic strain of the 1944 Tonankai earthquake [*Park et al.*, 2002]. The spatial correlation between the seaward limit of the 1958 earthquake rupture zone (Figure 8), the splay fault, and the conspicuous seafloor bulge suggests that the outer basement high had remained coupled to the downgoing plate during the preseismic and coseismic periods so that it had behaved as a deformable frontal buttress controlling the seaward rupture propagation along the splay fault. In this scenario, the rupture propagation would have produced instantaneous seafloor uplift above the splay fault, thus designating the shallow seafloor doming/graben area of the outer basement high as the primary tsunamogenic source during the 1958 earthquake.

5.4. Decoupling the Interplate Slip Across a Margin Wedge Transverse Fault

[29] Cross margin elastic stress accumulates irregularly along subduction zones as indicated by the distribution and timing of great subduction ruptures along the south American margin [*Kelleher*, 1972] and by the complex distribution of asperities in a single rupture zone [*Lay et al.*, 1982]. Geodetic or tide gage data from Chile [*Barrientos and Plafker*, 1992], Japan-Nankai [*Hyndman et al.*, 1995], and Alaska [*Savage and Plafker*, 1991] show that during interseismic periods, elastic strain accumulates across large regions of the forearc producing shortening and subsidence above the interplate locked zone and uplift landward. GPS measurements along the Ecuador margin (Figure 11) indicate elastic strain accumulation, supporting a locked portion of the plate interface [*Trenkamp et al.*, 2002; *White et al.*, 2003]. During the coseismic rupture, the pattern of deformation approximately reverses [*Hyndman and Wang*, 1995], producing uplift and forward rebound above the previously locked zone, and subsidence further landward. In the asperity model of *Lay et al.* [1982], the interplate fault zone is held by a discrete distribution of high strength asperities separated by weak zones. Failure of one asperity produces a rupture, which propagates through the neighboring weak zones and is pinned at both ends by adjacent asperities. Although asperities can physically relate to subducting seamounts [*Cloos*, 1992; *Cloos and Shreve*, 1996] or possible variations in sediment input, fluid content and pressure gradient along the subduction channel [*Cloos and Shreve*, 1988], physical characteristics proper to each margin segment may place additional stress on the coseismic slip area. According to wide-angle velocities [*Agudelo et al.*, 2002], the thickness of the margin basement appears to decrease from ~10 km on line SIS-35 to ~7 km on lines SIS-44 and SIS-45, 30–35 km from the trench. Such basement thinning accompanied by a 1- to 3-km thickening of overlying low-velocity sediment may contribute to variable interplate lithostatic pressure across the Manglares fault. Because the margin basement is a mosaic of heterogeneous, tectonically accreted oceanic blocks [*Baldock*, 1983; *Reynaud et al.*, 1999], its physical properties are expected to vary across the oceanic terranes, and influence the margin strength and interplate friction as well.

[30] In addition to downgoing plate structures and physical parameters of individual margin segments, a major tectonic structure transverse to the margin may equally delimit the coseismic slip zone by partially decoupling a fault block from adjoining sections of the fault [*Kelleher and Savino*, 1975]. Such a process depends on the relative fault strength and local stress field. Decoupling is likely to occur when the strength of the transverse fault is less than that of the plate interface. Thus the fault may act as a mechanical discontinuity to coseismic elastic rebound. Decoupling is also favored if the fault orientation is near that of the regional stress field. The N106°E orientation of the Manglares fault relative to the plate convergence vector [*Trenkamp et al.*, 2002] provides a smaller normal stress than that at the N150°E trending Esmeraldas fault, supporting an easier decoupling at the Manglares fault.

[31] In the simple transverse fault model of Figure 13a, all margin segments store elastic strain during the interseismic period. Coseismic slip then releases elastic strain and it propagates along the plate interface to the weak transverse fault zones F and G. Because of their low strength and stress field orientation, the faults prevent interplate elastic strain from propagating into the adjacent margin segments, which remain coupled and continue to accumulate strain until the next great subduction earthquake. We suggest that the transverse faults F and G in Figure 13a accommodated the coseismic elastic rebound with respectively a dextral and a sinistral strike-slip component. In the case of the 1958 earthquake rupture, the presence of the outer basement high and the interpreted megathrust splay fault added an outer structural constraint on the rupture propagation. Rupture of the 1958 asperity propagated north up to the Manglares fault (Figure 13b), where intense and very localized aftershock activity (Figure 2) implies high stress concentration at the plate interface [*Mendoza and Dewey*, 1984]. Because elastic strain accumulation decreases landward across the

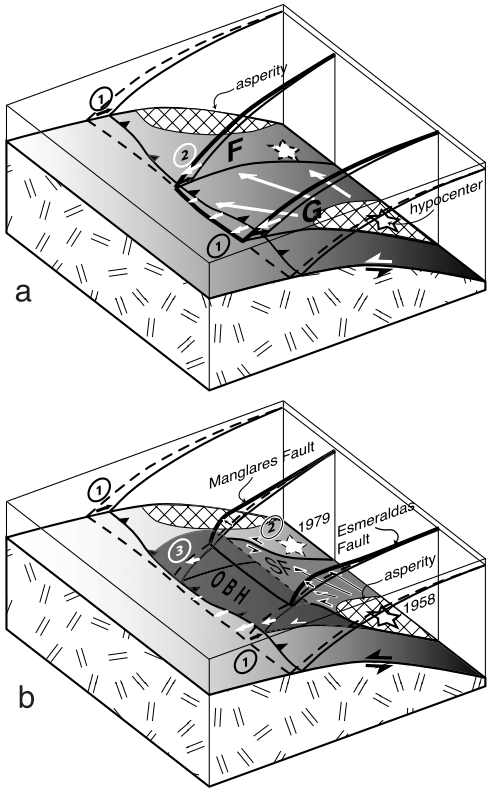

Figure 13. Schematic diagrams of the proposed rupture process of a subduction earthquake, controlled by crustal faults transverse to the margin. (a) Transverse faults extend to the margin front. In step 1, all three segments of the margin store irregularly elastic strain. In step 2, rupture initiates beneath central segment and coseismic slip propagates along the plate interface releasing elastic strain until it encounters the weak transverse faults. The faults act as mechanical barriers allowing the adjacent margin segment to remain locked. (b) During step 2, the 1958 coseismic slip propagated along the megathrust splay fault (SF) and locally uplifted the margin seafloor, possibly triggering the associated tsunami. Weak transverse faults, which may not extend to the deformation front, stop lateral propagation of the coseismic slip, allowing stress to increase in the adjacent margin segment and preparing for the 1979 rupture. In step 3, to compensate for thrust motion along the splay fault, the interplate décollement beneath the outer basement high (OBH) must have been activated by slow slip during the postseismic period.

margin [*Hyndman et al.*, 1995], only the seaward part of the fault is expected to have moved dextrally during the 1958 coseismic slip. Decoupling across the seaward part of the Manglares fault allowed continued elastic strain to build up in the adjacent margin segment, which failed during the great 1979 earthquake. We anticipate that the elastic rebound of the 1979 earthquake reactivated the Manglares fault with left-lateral motion. The behavior of the Esmeraldas fault during coseismic elastic rebound may significantly differ from that of the Manglares fault because of both its different orientation and proximity to the 1958 asperity. The Esmeraldas fault $\sim 60^\circ$ trend relative to the plate convergence vector partially impeded its expected left-lateral motion during rupture of the 1958 block (Figure 11). The resulting relative blocking combined with the fault proximity to the region of 1958 maximum coseismic slip (Figure 2), and presence of the resistant outer basement high, may have favored the splay fault development. Conversely, the Esmeraldas fault is likely to be more easily activated with a right-lateral sense of motion when the 1942 margin block is ruptured.

[32] Coseismic slip in 1958 appears to have been guided seaward by the splay fault and stopped beneath the outer rise (Figure 8). However, because the thrust splay fault does not offset the seafloor, we consider that the cumulative shortening along the fault is relatively small. We thus infer either that deformation is recent, which is not supported by the interpreted basin chronostratigraphy, or more likely that during the postseismic period, aseismic or slow slip occurs along the décollement underlying the outer basement high to compensate for thrust motion along the splay fault. We conclude that the great 1958 rupture zone was controlled by margin wedge structures and an asperity along the plate interface.

6. Conclusions

[33] MCS data reveal the deep structure and a transverse segmentation of the northern Ecuador– SW Colombia margin wedge, and the correlation of segment boundaries with the limits of the 1942, 1958 and 1979 interplate coseismic rupture zones.

[34] 1. We find evidence for the offshore continuation of the Jama Quininde and Esmeraldas crustal faults, defining a $\sim$200-km-long margin crustal block. The block extremities correlate with the lateral limits of the 1942 earthquake rupture zone, and the Jama Quininde fault is associated with the inferred southern limit of the great 1906 rupture zone. However, subduction of the thick, buoyant Carnegie Ridge is interpreted to partially lock the plate interface along central Ecuador so that the subducted ridge northern flank would have contributed to blocking the coseismic slip propagation for earthquakes of magnitude up to M_w 8.8, such as the 1906 event.

[35] 2. The N106°E trending Manglares fault is identified as a crustal transfer fault between a strongly shortened and uplifted margin segment north of the fault, and a poorly deformed and subsiding segment south of it. The fault likely coincides with the limit between the 1958 and 1979 rupture zones. Although the fault is not associated with a plate interface seismological asperity, it correlates with a zone of high interplate stress accumulation. These observations support the inhomogeneous barrier model of *Aki* [1979], which refers to the termination of earthquake rupture, where no obvious geometric discontinuity exists.

[36] 3. An outer seafloor and basement rise, as well as an interpreted mega thrust splay fault, coincide spatially with the seaward limit of the 1958 earthquake rupture zone, suggesting that the splay fault accommodated the 1958 coseismic elastic slip, and subsequent seafloor uplift was the main source of the associated tsunami.

[37] 4. A schematic three-dimensional transverse fault model that accounts for fault-bounded, coseismic slip propagation is proposed. In the model, adjacent margin segments irregularly store elastic strain. A transverse crustal

fault, oriented subparallel to the stress field and with a friction lower than that of the plate interface, is considered as a weak mechanical barrier to elastic strain release along strike the margin wedge. The seaward section of the fault should alternatively be reactivated by right- and left-lateral motion during successive subduction earthquakes rupturing adjacent margin segments.

[38] 5. We conclude that during the elastic rebound following a subduction earthquake of magnitude up to M_w 7.7, a weak subvertical transverse fault, properly oriented, can decouple adjacent margin segments, thus placing a limit on the lateral propagation of the coseismic slip.

[39] **Acknowledgments.** We are grateful to the Institut de Recherche pour le Développement (IRD), the Centre National de la Recherche Scientifique (CNRS), the Université Pierre et Marie Curie, and the GEOMAR Data Processing Center through the European Community (contract HPRI-CT-1999-00037) for funding and to IFREMER and GENAVIR for providing ship time, seismic equipment, and technicians. We thank the French Embassies in Bogota and Quito for help in obtaining research permits and for other logistics; G. Westbrook for kindly providing us with GLORIA data from the Charles Darwin cruise 40; and N. Bethoux, R. von Huene, P. Huchon, and G. Abers for helpful reviews. Maps were generated using GMT software [*Wessel and Smith*, 1998]. UMR 082-6526 Geosciences Azur contribution 671.

References

Abe, K. (1979), Size of great earthquakes of 1837–1974 inferred from tsunami data, *J. Geophys. Res.*, *84*, 1561–1568.

Agudelo, W., P. Charvis, J.-Y. Collot, B. Marcaillou, and F. Michaud (2002), Structure of the southwestern Colombia convergent margin from the SISTEUR seismic reflection-refraction experiment, paper presented at EGS XXVII General Assembly, Eur. Geophys. Soc., Nice, France.

Aki, K. (1979), Characterization of barriers on an earthquake fault, *J. Geophys. Res.*, *84*, 6140–6148.

Baldock, J. W. (1983), The northern Andes: A review of the Ecuadorian Pacific Margin, in *The Ocean Basins and Margins: The Pacific Ocean*, edited by A. E. Nairn, F. G. Stehli, and S. Uyeda, pp. 181–217, Plenum, New York.

Barrientos, S. E., and G. Plafker (1992), Postseismic coastal uplift in southern Chili, *Geophys. Res. Lett.*, *19*, 701–704.

Beck, S. L., and L. J. Ruff (1984), The rupture process of the great 1979 Colombia earthquake: Evidence for the asperity model, *J. Geophys. Res.*, *89*, 9281–9291.

Bilek, S. L., S. Y. Schwartz, and H. R. DeShon (2003), Control of seafloor roughness on earthquake rupture behavior, *Geology*, *31*(5), 455–458.

Cloos, M. (1992), Thrust-type subduction-zone earthquakes and seamount asperities: A physical model for seismic rupture, *Geology*, *20*, 601–604.

Cloos, M., and R. L. Shreve (1988), Subduction-channel model of prism accretion, melange formation, sediment subduction, and subduction erosion at convergent plate margins: 2. Implications and discussion, *Pure Appl. Geophys.*, *128*(3/4), 501–545.

Cloos, M., and R. L. Shreve (1996), Shear-zone thickness and seismicity of Chilean- and Marianas-type subduction zones, *Geology*, *24*(2), 107–110.

Collot, J.-Y., P. Charvis, M. A. Gutscher, and S. Operto (2002), Exploring the Ecuador-Colombia active margin and inter-plate seismogenic zone, *Eos Trans. AGU*, *83*(17), 189–190.

Cummins, P. R., T. Baba, S. Kodaira, and Y. Kaneda (2002), The 1946 Nankai earthquake and segmentation of the Nankai Trough, *Phys. Earth Planet. Inter.*, *132*, 75–87.

Daly, M. (1989), Correlations between Nazca/Farallon plate kinematics and forearc basin evolution in Ecuador, *Tectonics*, *8*, 769–790.

Deniaud, Y. (2000), Enregistrements sédimentaire et structural de l'évolution géodynamique des Andes Equatoriennes au cours du Néogène: Etude des bassins d'avant-arc et bilans de masse, Ph.D. thesis, Univ. Joseph Fourier, Grenoble, France.

Dominguez, S., S. Lallemand, J. Malavieille, and R. von Huene (1998), Upper plate deformation associated with seamount subduction, *Tectonophysics*, *293*, 207–224.

Duque-Caro, H. (1990), The Choco block in the northwestern corner of south Alerica: Structural, tectonostratigrahic and paleogeographic implications, *J. S. Am. Earth Sci.*, *3*, 71–84.

Espinoza, J. (1992), Terremotos tsunamigenicos en el Ecuador, *Acta Oceanogr. Pac.*, *7*(1), 21–28.

Evans, C. D. R., and J. E. Wittaker (1982), The geology of the western part of the Borbon Basin, northwest Ecuador, in *Trench-Forearc Geology: Sedimentation and Tectonics on Modern and Ancient Active Plate Margins*, edited by J. K. Leggett, *Geol. Soc. Spec. Publ.*, *10*, 191–200.

Graindorge, D., A. Calahorrano, P. Charvis, J.-Y. Collot, and N. Bethoux (2004), Deep structures of the Ecuador convergent margin and the Carnegie Ridge, possible consequence on great earthquakes recurrence interval, *Geophys. Res. Lett.*, *31*, L04603, doi:10.1029/2003GL018803.

Gutscher, M. A., J. Malavieille, S. Lallemand, and J. Y. Collot (1999), Tectonic segmentation of the North Andean margin: Impact of the Carnegie Ridge collision, *Earth Planet. Sci. Lett.*, *168*, 255–270.

Herd, D. G., T. L. Youd, H. Meyer, J. L. Arango C., W. J. Person, and C. Mendoza (1981), The Great Tumaco, Colombia earthquake of 12 December 1979, *Science*, *211*, 441–445.

Husen, S., E. Kissling, and R. Quintero (2002), Tomographic evidence for a subducted seamount beneath the Gulf of Nicoya, Costa Rica: The cause of the 1990 M_w = 7.0 Gulf of Nicoya earthquake, *Geophys. Res. Lett.*, *29*(8), 1238, doi:10.1029/2001GL014045.

Hyndman, R. D., and K. Wang (1995), The rupture zone of the Cascadia great earthquakes from current deformation and the thermal regime, *J. Geophys. Res.*, *100*, 22,133–22,154.

Hyndman, R. D., K. Wang, and M. Yamano (1995), Thermal constraints on the seismogenic portion of the southwestern Japan subduction thrust, *J. Geophys. Res.*, *100*, 15,373–15,392.

Kanamori, H. (1986), Rupture process of subduction zone earthquakes, *Annu. Rev. Earth Planet. Sci.*, *14*, 293–322.

Kanamori, H., and J. W. Given (1981), Use of long-period surface waves for rapid determination of earthquake-source parameters, *Phys. Earth Planet. Inter.*, *27*, 8–31.

Kanamori, H., and K. C. McNally (1982), Variable rupture mode of the subduction zone along the Ecuador-Colombia coast, *Bull. Seismol. Soc. Am.*, *72*(4), 1241–1253.

Kelleher, J. (1972), Rupture zones of large South American earthquakes and some predictions, *J. Geophys. Res.*, *77*, 2087–2103.

Kelleher, J., and W. McCann (1976), Buoyant zones, great earthquakes, and unstable boundaries of subduction, *J. Geophys. Res.*, *81*, 4885–4896.

Kelleher, J., and J. Savino (1975), Distribution of seismicity before large strike-slip and thrust-type earthquakes, *J. Geophys. Res.*, *80*, 260–271.

Kodaira, S., N. Takahashi, A. Nakanishi, S. Miura, and Y. Kaneda (2000), Subducted seamount imaged in the rupture zone of the 1946 Nankaido earthquake, *Sciences*, *289*, 104–106.

Lay, T., H. Kanamori, and L. Ruff (1982), The asperity model and the nature of large subduction zone earthquakes, *Earthquake Predict. Res.*, *1*, 3–71.

Lonsdale, P. (1978), Ecuadorian Subduction System, *AAPG Bull.*, *62*(12), 2454–2477.

Lonsdale, P., and K. D. Klitgord (1978), Structure and tectonic history of the eastern Panama Basin, *Geol. Soc. Am. Bull.*, *89*, 981–999.

Marcaillou, B. (2003), Régimes tectoniques et thermiques de la marge Nord Equateur- Sud Colombie (0°–3.5°N)—Implications sur la sismogenèse, Ph.D. thesis, Univ. Pierre et Marie Curie, Paris.

McCaffrey, R. (1993), On the role of the upper plate in great subduction zone earthquakes, *J. Geophys. Res.*, *98*, 11,953–11,966.

Mendoza, C., and J. W. Dewey (1984), Seismicity associated with the great Colombia-Ecuador earthquakes of 1942, 1958 and 1979: Implications for barrier models of earthquake rupture, *Bull. Seismol. Soc. Am.*, *74*(2), 577–593.

Moberly, R., G. L. Shepherd, and W. T. Coulbourn (1982), Forearc and other basins, continental margin of northern and southern Peru and adjacent Ecuador and Chile, in *Trench-Forearc Geology: Sedimentation and Tectonics on Modern and Ancient Active Plate Margins*, edited by J. K. Leggett, *Geol. Soc. Spec. Publ.*, *10*, 245–258.

Mogi, K. (1969), Relationship between the occurrence of great earthquakes and tectonic structures, *Bull. Earthquake Res. Inst.*, *47*, 429–451.

Moore, J. C., and D. Saffer (2000), Up-dip limit of the seismogneic zone beneath the accretionary prism of southwest Japan: An effect of diagenetic to low-grade metamorphic processes and increasing effective stress, *Geology*, *29*, 183–186.

Pacheco, J. F., L. R. Sykes, and C. H. Scholz (1993), Nature of seismic coupling along simple plate boundaries of the subduction type, *J. Geophys. Res.*, *98*, 14,133–14,159.

Park, J.-O., T. Tsuru, S. Kodaira, P. R. Cummins, and Y. Kaneda (2002), Splay fault branching along the Nankai subduction zone, *Science*, *297*, 1157–1160.

Pedoja, K. (2003), Les terrasses marines de la marge nord andine (Equateur-Nord Pérou): Relations avec le contexte géodynamique, Ph.D. thesis, Univ. Pierre et Marie Curie, Paris.

Reynaud, C., E. Jaillard, H. Lapierre, M. Mamberti, and G. H. Mascle (1999), Oceanic plateau and island arcs of southwestern Ecuador: Their

place in the geodynamic evolution of northwestern South America, *Tectonophysics*, *307*, 235–254.

Ruff, L. J., and H. Kanamori (1983), The rupture process and asperity distribution of three great earthquakes from long-period diffracted *P*-waves, *Phys. Earth Planet. Inter.*, *31*, 202–230.

Sallares, V., P. Charvis, E. R. Flueh, J. Bialas, and C. Wahlter (2002), Wide-angle seismic constraints on the evolution of Galapagos hotspot-Cocos-Nazca spreading center interaction, paper presented at EGS XXVII General Assembly, Eur. Geophys. Soc., Nice, France.

Sandwell, D. T., and W. H. F. Smith (1994), New global marine gravity map/grid based on stacked ERS-1, Geosat and Topex altimetry, *Eos Trans. AGU*, *75*(16), Spring Meet. Suppl., S321.

Santana, E., and J. F. Dumont (2002), The San Lorenzo fault, a new active fault in relation to the Esmeraldas-Tumaco seismic zone, paper presented at 5th International Symposium on Andean Geodynamics, IRD, Univ. Paul Sabatier, Toulouse, France.

Savage, J. C., and G. Plafker (1991), Tide gage measurements of uplift along the south coast of Alaska, *J. Geophys. Res.*, *96*, 4325–4335.

Scholz, C. H. (1988), The brittle-ductile transition and the depth of seismic faulting, *Geol. Rundsch.*, *77*, 319–328.

Scholz, C. H., and C. Small (1997), The effect of seamount subduction on seismic coupling, *Geology*, *25*, 487–490.

Shipboard Scientific Party (2002), Leg 202 preliminary report, southeast Pacific paleoceanographic transects, Ocean Drill. Program, Tex. A&M Univ., College Station, Tex.

Stauder, W. (1972), Fault motion and spatially bounded character of earthquakes in Amchitka pass and the Delarof islands, *J. Geophys. Res.*, *77*, 2072–2080.

Swenson, J. L., and S. L. Beck (1996), Historical 1942 Ecuador and 1942 Peru subduction earthquakes, and earthquake cycles along Colombia-Ecuador and Peru subduction segments, *Pure Appl. Geophys.*, *146*(1), 67–101.

Sykes, L. R. (1971), Aftershock zones of great earthquakes, seismicity gaps, and earthquake prediction for Alaska and the Aleutians, *J. Geophys. Res.*, *76*, 8021–8041.

Taboada, A., L. A. Rivera, A. Fuenzalida, A. Cisternas, H. Philip, H. Bijwaard, and J. Olaya (2000), Geodynamics of the northern Andes: Subductions and intracontinental deformation (Colombia), *Tectonics*, *19*, 787–813.

Thatcher, W. (1990), Order and diversity in the modes of circum-Pacific earthquake recurrence, *J. Geophys. Res.*, *95*, 2609–2623.

Trenkamp, R., J. N. Kellogg, J. T. Freymueller, and P. Mora (2002), Wide plate margin deformation, southern Central America and northwestern South America, CASA GPS observations, *J. S. Am. Earth Sci.*, *15*, 157–171.

Vrolijk, P. (1990), On the mechanical role of smectite in subduction zones, *Geology*, *18*, 703–707.

Wang, K., R. D. Hyndman, and M. Yamano (1995), Thermal regime of the southwest Japan subduction zone: Effects of age history of the subducting plate, *Tectonophysics*, *248*, 53–69.

Wessel, P., and W. D. Smith (1998), New, improved version of Generic Mapping Tools released, *Eos Trans. AGU*, *79*(47), 579.

Westbrook, G. K., N. C. Hardy, and R. P. Heath (1995), Structure and tectonics of the Panama-Nazca plate boundary, *Spec. Pap. Geol. Soc. Am.*, *295*, 91–109.

White, S. M., R. Trenkamp, and J. N. Kellogg (2003), Recent crustal deformation and the earthquake cycle along the Ecuador-Colombia subduction zone, *Earth Planet. Sci. Lett.*, *216*, 231–242.

Zamora, A., et al. (1993), Mapa Geologico de la Republica del Ecuador, Brit. Geol. Surv., Keyworth, U.K.

W. Agudelo, D. Graindorge, B. Marcaillou, F. Michaud, and F. Sage, Geosciences Azur, Université Pierre et Marie Curie (UPMC), BP 48, F-06235 Villefranche sur Mer, France.

P. Charvis and J.-Y. Collot, Geosciences Azur, Institut de Recherche pour le Développement (IRD), BP 48, F-06235 Villefranche sur Mer, France. (collot@geoazur.obs-vlfr.fr)

M.-A. Gutscher, Centre National de la Recherche Scientifique (CNRS), Université de Bretagne Occidentale, UMR 6538 Domaines Oceaniques, Place Nicolas Copernic, F-29280, Plouzane, France.

G. Spence, School of Earth and Ocean Sciences, University of Victoria, PO Box 3055 STN CSC, Victoria, British Columbia, Canada V8W 3P6.

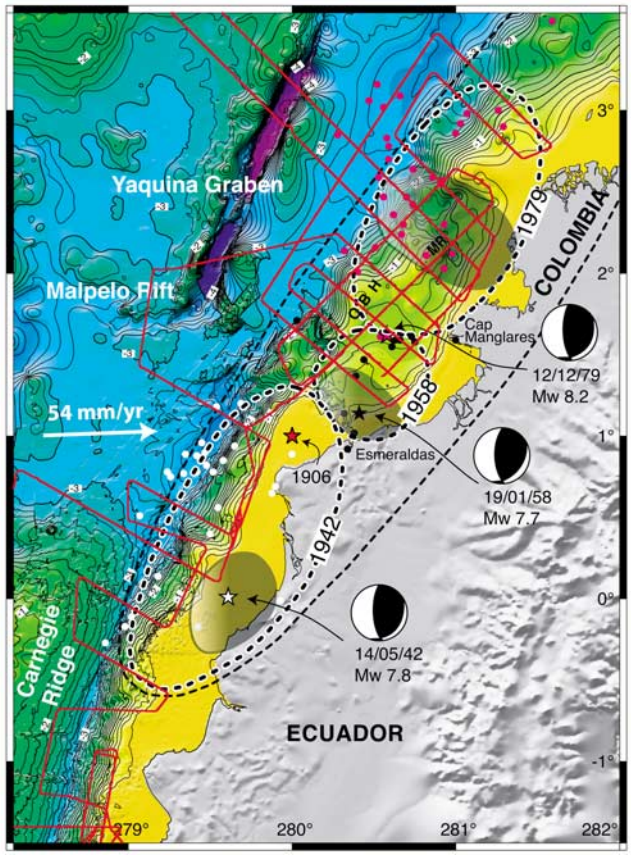

Figure 2. Location of the 20th century great subduction earthquake rupture zones of northern Ecuador–SW Colombia (dashed ellipses), epicenters (stars), and their associated relocated 3-month aftershocks of $m_b > 4.8$ (white, black, and red dots) [*Mendoza and Dewey*, 1984], seismological asperities (gray shaded elliptic areas) and focal mechanisms [*Kanamori and Given*, 1981; *Kanamori and McNally*, 1982; *Swenson and Beck*, 1996; *Herd et al.*, 1981; *Beck and Ruff*, 1984]. Bathymetry map in km has been compiled from NGDC and the R/V *Nadir* SISTEUR cruise single beam bathymetric data (red lines) and swath bathymetry from the R/V *l'Atalante* Pugu cruise and the R/V *Sonne* Salieri and SO162 cruises. OBH is outer basement high; MR is middle ridge. Open arrow shows Nazca–South America relative plate motion vector, derived from *Trenkamp et al.*'s [2002] GPS study.